Motion of a Distinguishable Impurity in the Bose Gas

Arrested Expansion Without a Lattice and Impurity Snaking

Robinson, N.J.; Caux, J.-S.; Konik, R.M.

DOI
10.1103/PhysRevLett.116.145302

Publication date
2016

Document Version
Other version

Published in
Physical Review Letters

Supplemental Materials for "Motion of a distinguishable impurity in the Bose gas: Arrested expansion without a lattice and impurity snaking'

Neil J. Robinson,[1,2,*] Jean-Sébastien Caux,[3] and Robert M. Konik[1]

[1] *CMPMS Dept., Brookhaven National Laboratory, Upton, NY 11973-5000, USA*
[2] *The Rudolf Peierls Centre for Theoretical Physics, University of Oxford, Oxford, OX1 3NP, United Kingdom*
[3] *Institute for Theoretical Physics, University of Amsterdam, Science Park 904, Postbus 94485, 1090 GL Amsterdam, The Netherlands*

(Dated: March 3, 2016)

A. Summary of required matrix elements for the two-component Lieb-Liniger model

Here we summarize known results[1] for matrix elements of local operators in the two-component Lieb-Liniger model. For technical reasons, the known matrix elements of Ref. [1] are restricted to the case with a single impurity boson ($N_1 = 1$) and to the local operators $\Psi_1(0)$, $\Psi_1^\dagger(0)\Psi_1(0)$ and $\Psi_1^\dagger(0)\Psi_2(0)$. As a consequence of this, we are not able to 'image' the background gas $\Psi_2^\dagger(0)\Psi_2(0)$. Very recently[2] there have been new (and more general) results for matrix elements in the two-component Lieb-Liniger model, but we have yet implement them.

1. *Normalization conventions*

We focus on N-particle eigenstates containing a single N_1 boson. For clarity and ease of comparison, here we work with the conventions of Ref. [3] and we define the (non-normalized) eigenstates $|\{q\}_N;\mu\rangle\rangle$. The eigenstates in the body of the text are recovered by normalization $|\{q\}_N;\mu\rangle = |\{q\}_N;\mu\rangle\rangle/||\{q\}_N;\mu||$, where norms of the eigenstates are given by

$$||\{q\}_N;\mu||^2 = \langle\langle\{q\}_N;\mu|\{q\}_N;\mu\rangle\rangle = c\,\det\mathcal{J}_2,$$
$$\mathcal{J}_2 = \begin{pmatrix} J_{qq} & J_{q\mu} \\ J_{\mu q} & J_{\mu\mu} \end{pmatrix}.$$

Here $\mathcal{J}_2$ is the Jacobian of the nested Bethe ansatz equations [see Eqs. (2,3)] given by the matrix elements

$$\begin{aligned}(J_{qq})_{jl} &= \delta_{jl}\left[L + \sum_{m=1}^{N}\varphi_1(q_j - q_l) - \varphi_2(q_m - \mu)\right] \\ &\quad -\varphi_1(q_j - q_l), \\ (J_{q\mu})_{j1} &= (J_{\mu q})_{1j} = \varphi_2(k_j - \mu), \\ J_{\mu\mu} &= \sum_{m=1}^{N}\varphi_2(k_m - \mu),\end{aligned}$$

where we define the scattering phase $\varphi_n(u) = 2cn/(n^2u^2 + c^2)$ and $j, l = 1, \ldots, N$.

We take the one-component Lieb-Liniger eigenstates $|\{p\}_N\rangle\rangle$ to have their conventional normalization[4–7]

$$||\{p\}_N||^2 = \prod_{j<l}\Big[(p_j - p_l)^2 + c^2\Big]\det\mathcal{J}_1,$$
$$(\mathcal{J}_1)_{jl} = \delta_{j,l}\left[L + \sum_{m=1}^{N}\varphi_1(p_j - p_m)\right] - \varphi_1(p_j - p_l).$$

2. *Matrix elements* $\langle\langle\{p\}_N|\Psi_1(0)|\{k\}_N;\lambda\rangle\rangle$

For two states with no coinciding momenta, the matrix element of the impurity annihilation operator takes the determinant form

$$\begin{aligned}&\langle\langle\{p\}_{N-1}|\Psi_1(0)|\{k\}_N;\lambda\rangle\rangle \\ &= \frac{\prod_{i>j}(k_i - k_j + ic)}{\prod_{l>m}(p_l - p_m + ic)}\frac{-ic}{\prod_j(\lambda - k_j - ic/2)}\det\mathbb{M}.\end{aligned}$$

Here the $(N-1)\times(N-1)$ matrix $\mathbb{M}$ has elements $\mathbb{M}_{jk} = M_{jk} - M_{N,k}$ with

$$\begin{aligned}M_{jk} = t(p_k - k_j)h_2(\lambda - k_j)\frac{\prod_{m=1}^{N-1}h_1(p_m - k_j)}{\prod_{m=1}^{N}h_1(k_m - k_j)} \\ +t(k_j - p_k)h_2(k_j - \lambda)\frac{\prod_{m=1}^{N-1}h_1(k_j - p_m)}{\prod_{m=1}^{N}h_1(k_j - k_m)}\end{aligned}$$

where we've defined the functions $h_n(u) = u + ic/n$ and $t(u) = -c/[u(u + ic)]$.

3. *Matrix elements* $\langle\langle\{p\}_N;\mu|\Psi_1^\dagger(0)\Psi_1(0)|\{k\}_N;\lambda\rangle\rangle$

For two states with no coinciding momenta, the matrix elements of the impurity density operator are

$$\begin{aligned}&\langle\langle\{p\}_N;\mu|\Psi_1^\dagger(0)\Psi_1(0)|\{k\}_N;\lambda\rangle\rangle \\ &= \frac{-i}{c}(-1)^{N(N+1)/2}\prod_{j>l}\frac{1}{k_j - k_l - ic}\prod_{j>l}\frac{1}{p_j - p_l + ic}\det\mathbb{V} \\ &\times\prod_{l,m=1}^{N}\Big(k_l - p_m + ic\Big)\frac{c^2}{\prod_j(\lambda - k_j - ic/2)(\mu - p_j + ic/2)}\end{aligned}$$

where the $(N+1)\times(N+1)$ matrix $\mathbb{V}$ has elements

$$\begin{aligned}\mathbb{V}_{jl} &= \left(p_l-\lambda+\frac{ic}{2}\right)\left(p_l-\mu-\frac{ic}{2}\right)\tilde{t}(k_j-p_l)\\ &+\left(p_l-\lambda-\frac{ic}{2}\right)\left(p_l-\mu+\frac{ic}{2}\right)\tilde{t}(p_l-k_j)\\ &\times\prod_{m=1}^{N}\frac{(p_l-k_m+ic)(p_l-p_m-ic)}{(p_l-k_m-ic)(p_l-p_m+ic)}\\ \mathbb{V}_{N+1,j} &= \prod_{m=1}^{N}\frac{p_m-p_j+ic}{k_m-p_j+ic},\qquad \mathbb{V}_{j,N+1}=1,\\ \mathbb{V}_{N+1,N+1} &= 0,\end{aligned}$$

with $j,l = 1,\ldots,N$. Additionally, the diagonal elements of the impurity density operator follow from translational invariance of the eigenstates: $\langle\{k\}_N;\lambda|\Psi_1^\dagger(0)\Psi_1(0)|\{k\}_N;\lambda\rangle = 1/L$.

B. Dynamics of an indistinguishable impurity in the one-component Lieb-Liniger model

Here we consider the initial state

$$|\Psi_2(Q)\rangle = \frac{1}{\mathcal{N}_2}\int_0^L \mathrm{d}x\; e^{iQx}e^{-\frac{1}{2}\left(\frac{x-x_0}{a_0}\right)^2}\Psi_2^\dagger(x)|\Omega\rangle, \quad \text{(S1)}$$

where $|\Omega\rangle$ is the ground state of N_2 bosons of species 2, e.g. the analogue of Eq. (4) with an indistinguishable impurity. We wish to consider the time evolution of the expectation value of the density operator $\Psi_2^\dagger(x)\Psi_2(x)$ with this initial state. Our prescription for computing the time evolution is analogous to the two-component case: we expand the expectation value $\rho_2(x,t) = \langle\Psi_2(Q,t)|\Psi_2^\dagger(x)\Psi_2(x)|\Psi_2(Q,t)\rangle$ in terms of known matrix elements and overlaps between the Bethe states,[3–10] to obtain an expansion similar to Eq. (5).

For the case with $Q=0$, we can gain some insight from examining the noninteracting limit $c=0$. Working on the infinite system ($L\to\infty$) with $x_0=0$, we find the density

$$\begin{aligned}\rho_2(x,t) = \rho + \frac{a_0^2}{\sqrt{\pi a_0^2+2\pi a_0^2\rho}}\Bigg[&\frac{e^{-\frac{a_0^2x^2}{a_0^4+4t^2}}}{\sqrt{a_0^4+4t^2}}\\ &+\rho\sqrt{2\pi}\frac{e^{-\frac{a_0^2}{2}\frac{x^2}{a_0^4+4t^2}}}{(a_0^4+4t^2)^{\frac{1}{4}}}\cos\left(\theta_t-\frac{tx^2}{a_0^4+4t^2}\right)\Bigg],\end{aligned} \quad \text{(S2)}$$

where ρ is the average density and with ρ and $2\theta_t = \arctan(2t/a_0^2)$. Thus we expect the wave packet to be of Gaussian shape with oscillations superimposed on top.

We present the time evolution of the density operator on the initial state (S1) for $N=8$ particles, $Q=0$, $a_0^2=1.125$ and $L=2x_0=40$ in Fig. S1. We see that the behavior of the density as it evolves in time is qualitatively consistent with the noninteracting result (S2). We see no evidence of a stalling of the spreading of the wave packet, which is not surprising as the mechanism which exists in the two-component case (hole formation in the background gas and subsequent trapping of the impurity in the hole) is not present when there is a single species of boson.

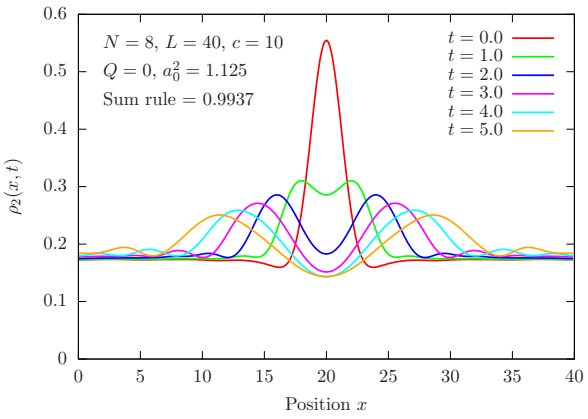

FIG. S1. Time evolution of the density profile $\rho_2(x,t)$ for the initial state (S1) in the one-component Lieb-Liniger model for $N=8$ particles on the circumference $L=40$ ring with interaction parameter $c=10$. We used 12619 states to saturate the sum rule to 0.9937.

C. Lattice mean field description

In an attempt to explain the dynamics of the initial state, Eq. (4) in the main text, we consider the following lattice Hamiltonian (we consider a lattice Hamiltonian for numerical convenience):

$$\begin{aligned}H_{\text{latt}} = &-J_d\sum_l\left(d_l^\dagger d_{l+1}+\text{H.c}\right)+U\sum_l\left(n_l^b+n_l^d\right)^2\\ &-J_b\sum_l\left(b_l^\dagger b_{l+1}+\text{H.c.}\right),\end{aligned} \quad \text{(S3)}$$

where $n_l^a = a_l^\dagger a_l$ is the number operator. This model is motivated by the two-component Lieb-Liniger model: we consider two species of bosons which have an on-site interaction only and the kinetic terms coincide in the continuum limit

$$\begin{aligned}\lim_{a_0\to0} d(x)^\dagger d(x+a_0) &\to d^\dagger(x)d(x)+a_0d^\dagger(x)\partial_x d(x)\\ &+\frac{a_0^2}{2}d^\dagger(x)\partial_x^2 d(x),\\ \sum_l d_l^\dagger d_{l+1}+d_l^\dagger d_{l-1} &\to \text{const.}+a_0\int\mathrm{d}x\; d^\dagger(x)\partial_x^2 d(x).\end{aligned}$$

We choose the d bosons to play the role of the background gas (species 2 in the main body of the manuscript) and

we consider $U \gg J_d$ to reflect the strong coupling regime of the main text.

The Heisenberg equations of motion for the boson bilinears take the form

$$\frac{\mathrm{d}}{\mathrm{d}t} b_i^\dagger b_j = -iJ_b\Big(b_{i-1}^\dagger b_j + b_{i+1}^\dagger b_j - b_i^\dagger b_{j+1} - b_i^\dagger b_{j-1}\Big) + iU\Big[b_i^\dagger b_j (n_i^b - n_j^b) + (n_i^b - n_j^b) b_i^\dagger b_j + 2(n_i^d - n_j^d) b_i^\dagger b_j\Big] \ ,$$

and similarly for $d_i^\dagger d_j$ with $d \leftrightarrow b$. We take the expectation value of this expression and perform a time-dependent mean-field decoupling which preserves the $U(1)$ symmetry for each of the species (cf. Eq. (7))

$$\langle (n_i^d - n_j^d) b_i^\dagger b_j\rangle \to \Big(\langle n_i^d(t)\rangle - \langle n_j^d(t)\rangle\Big)\langle b_i^\dagger(t) b_j(t)\rangle, \qquad \langle n_i^b(t) b_i^\dagger(t) b_j(t)\rangle \to \langle n_i^b(t)\rangle\langle b_i^\dagger(t) b_j(t)\rangle + \langle b_i^\dagger b_j(t)\rangle\langle b_i b_i^\dagger(t)\rangle,$$

to arrive at the *approximate* equations of motion for the boson bilinears:

$$\begin{aligned}\frac{\mathrm{d}}{\mathrm{d}t}\langle b_i^\dagger b_j(t)\rangle = &-iJ_b\Big[\langle b_{i-1}^\dagger b_j(t)\rangle - \langle b_i^\dagger b_{j+1}(t)\rangle + \langle b_{i+1}^\dagger b_j(t)\rangle - \langle b_i^\dagger b_{j-1}(t)\rangle\Big] \\ &+2iU\Big[\langle n_i^d(t)\rangle - \langle n_j^d(t)\rangle + 2\langle n_i^b(t)\rangle - 2\langle n_j^b(t)\rangle\Big]\langle b_i^\dagger b_j(t)\rangle, \end{aligned} \tag{S4}$$

with similar for the d bosons. Our initial conditions are fixed by the initial state $|\Psi(Q)\rangle$; for the purposes of convenience, we consider the ground state $|\Omega\rangle$ to be the $c = 0$ ground state (this is an approximation, alternatively one can view this situation as a combination of injecting the impurity and performing a quantum quench of the interaction parameter), in which only the zero-mode is populated. The initial conditions for the bilinears are:

$$\begin{aligned}\langle b_i^\dagger b_j\rangle_0 &= \frac{1}{|\mathcal{N}|^2} e^{-\frac{1}{2}\left(\frac{i-i_0}{a_0}\right)^2} e^{-\frac{1}{2}\left(\frac{j-i_0}{a_0}\right)^2} e^{iQ(i-j)}, \\ \langle d_i^\dagger d_j\rangle_0 &= \rho, \end{aligned} \tag{S5}$$

where $\rho = N/L$ is the density of the background gas and $|\mathcal{N}|^2 = \sum_x \exp[-(x-x_0)^2/a_0^2]$ is a normalization factor.

We present results for the expectation values of the density operators in Figs. S2 and S3 for $U = 14.5$ and $J_d = J_b = 1$ with $\rho = 0.2$ and $a_0 = 2$ on the circumference $L = 40$ ring. Parameters were chosen in an attempt to qualitatively reproduce the $Q = 0$ continuum behavior: arrested expansion followed by eventual spreading of the impurity (*cf.* Fig. S4). In Fig. S2 we see approximately the required behavior for $Q = 0$: the impurity initially spreads, but for times $t \sim t_F - 9t_F$ expansion is arrested (the nature of the amplitude and fluctuations is clearly very different in the mean field lattice case compared to the continuum) before subsequently spreading. In the background gas, Fig. S2(b), we see that a region of depleted density (a 'hole') appears below the impurity, which remains despite multiple collisions with propagating wave packets (the red peaks crisscrossing the figure).

In Fig. S3 we present similar data for the case with $Q = 13 \times (2\pi/L)$ (we move away from $Q = \pi$ as this is a special point in the lattice case). Surprisingly we see that the addition of finite center of mass momentum for the impurity has lead to a *strengthening* of the dynamical arrest in the mean field approximation, with a deep and more robust hole forming in the background gas. Clearly we see no evidence of the 'snaking' behavior observed in the continuum, despite multiple collisions with excitations in the background gas. This strongly suggests that the behavior observed in the continuum for $Q \neq 0$ is beyond mean field theory (and may differ dramatically to that observed on the lattice).

D. Addition plots: $Q = 0$ long time and $Q = 0, \pi$ constant-time cuts

Here we present additional data for the time-evolution of the initial state with $Q = 0$ and $Q = \pi$. In Fig. S4(a) we present the time-evolution for up to time $t \sim 20t_F$. As we saw in the main text, for times $2t_F \lesssim t \lesssim 7t_F$ the impurity undergoes arrested expansion: it is approximately stationary, with only small amplitude breathing oscillations. Following the arrested expansion, there is a period of rapid expansion, followed by a shorter quasistationary period and then subsequent expansion. In Fig. S4(b) we present constant time cuts for short times $t \leq 9$ ($t \lesssim 3.5t_F$) , which show the initial period of rapid expansion and subsequent arrested expansion. Figure S5 presents similar time cuts for the initial state with $Q = \pi$ for $c = 5, 10, 20$.

E. Quantum Newton's cradle on the ring

1. *Motion of the center of mass*

Here we provide support for our assertion that the motion of the center of mass coordinate can be explained in terms of a "quantum Newton's cradle" on the ring. The motion of the center of mass coordinate is presented in Fig. 3 of the manuscript, where we observe periods of rapid motion separated by approximately stationary

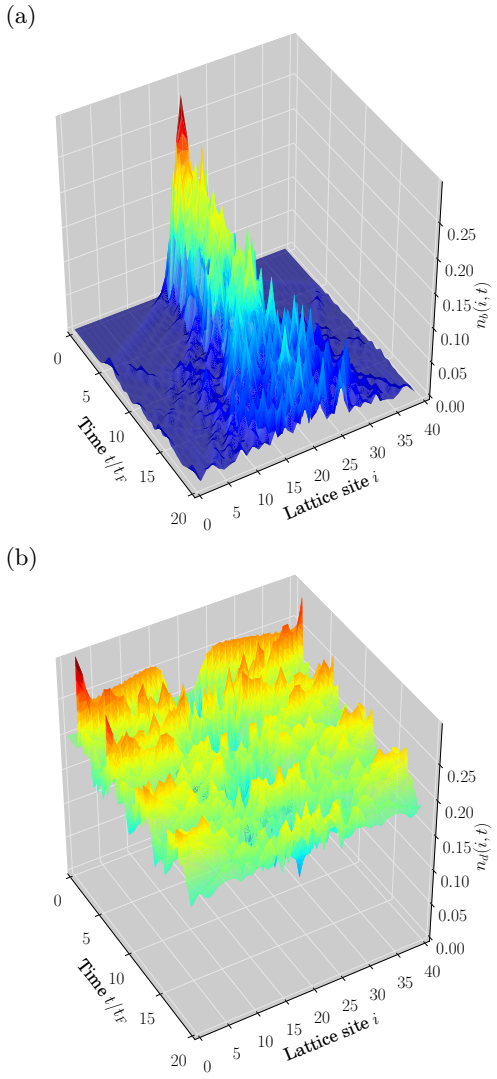

FIG. S2. Time depedence of the (a) n_b; (b) n_d boson number operator expectation values from the mean-field equations of motion (S4) with $U = 14.5$ and $J_d = J_b = 1$. Initial conditions (S5) with $a_0 = 2$, $Q = 0$ and $\rho = 0.2$ for $L = 40$ sites were used.

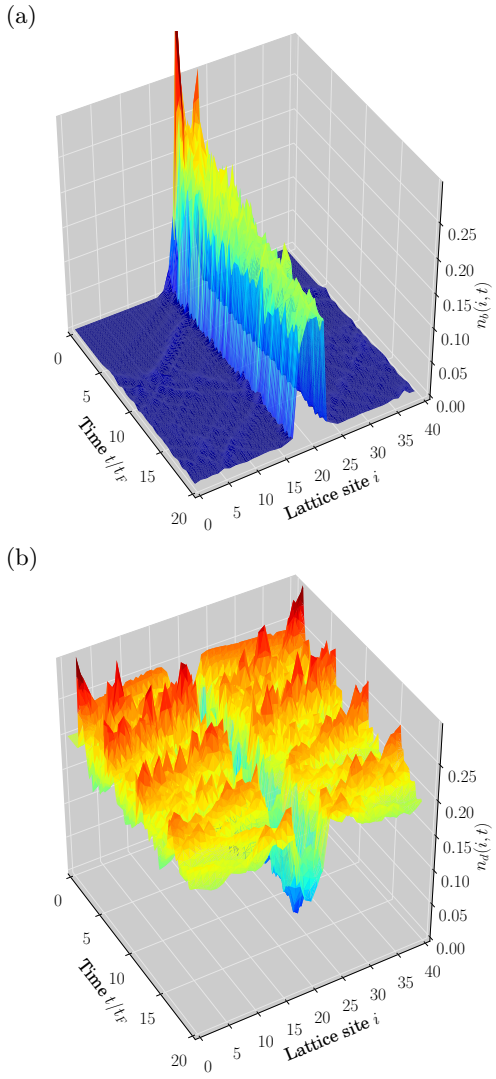

FIG. S3. Time depedence of the (a) n_b; (b) n_d boson number operator expectation values from the mean-field equations of motion (S4) with $U = 14.5$ and $J_d = J_b = 1$. Initial conditions (S5) with $a_0 = 2$, $Q = 13 \times 2\pi/L$ and $\rho = 0.2$ for $L = 40$ sites were used. .

plateaux (see also Figs. S5). We have the following explanation for the observed behavior: as the impurity moves through the background gas, it collides and excites the background gas, with the excitations predominantly moving in the same direction as the impurity. The impurity continues to collide with the background gas until it has imparted all (or most) of its center of mass momentum, and subsequently the center of mass coordinate is (approximately) stationary. The excitations in the background gas propagate around the ring, until they once again reach the impurity and collide with it, imparting momentum and causing the center of mass of the impurity to once more move. This process then repeats. In support of this picture, in Fig. S6(a) we present the center of mass motion in three systems with different sizes and fixed particle density (this means the speed of sound in the system should be similar, up to small finite size effects), and we see that the time for which the center of mass is stationary is linearly dependent on the system size L. In Fig. S6(b) we present the center of mass motion for four different initial momenta Q, and we see the length of the plateau is inversely proportional to Q at large Q (the velocity of an excitation with momentum Q is $v = Q/m$). Both of these results are consistent with the presented picture, where the deviation from the stationary plateau is driven by finite momentum excitations propagating around the ring.

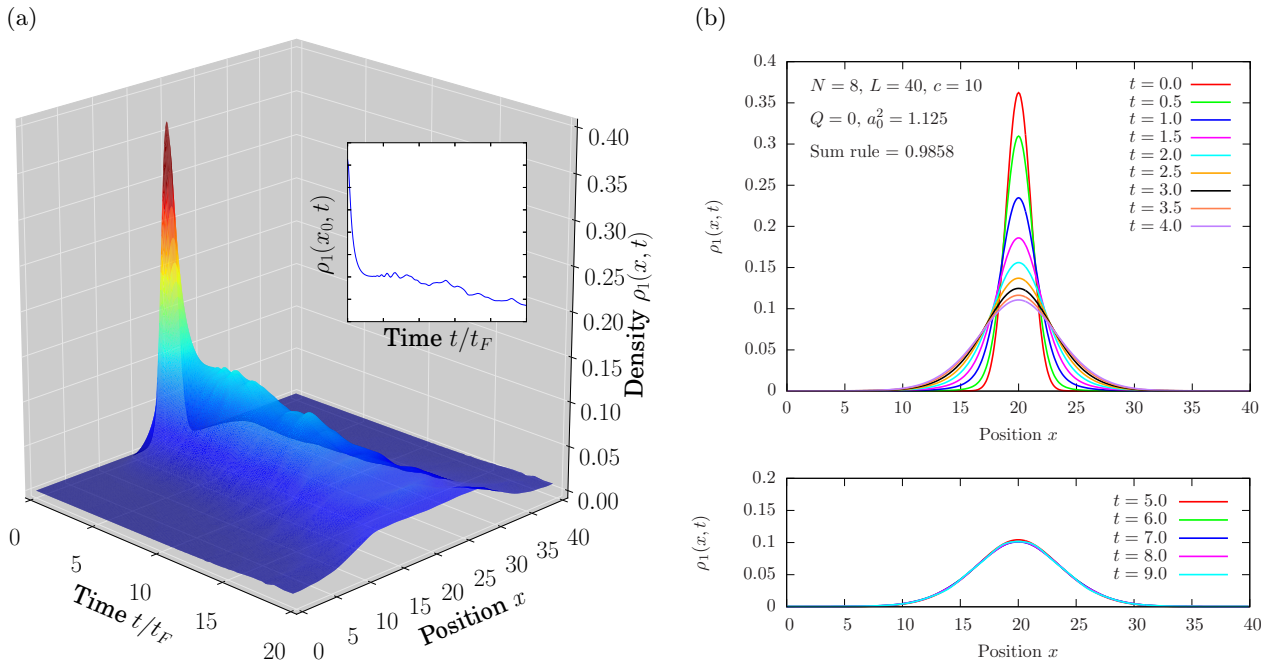

FIG. S4. Time evolution of the impurity density of the initial state $|\Psi(Q)\rangle$ [defined in Eq.(4)] with $Q = 0$, $x_0 = L/2$ and $a_0^2 = 1.125$ on the $L = 40$ ring for a system of $N = 8$ particles with interaction parameter $c = 10$. The Hilbert space is truncated to 25150 states, leading to the sum rule [Eq. (6)] $= 0.9858$. (a) The full time-evolution, showing the initial rapid expansion, followed by a period of arrested expansion and subsequent spreading/quasi-stationary periods. Inset is the time-evolution of the density at the midpoint. (b) Constant-time cuts at short times, showing in detail the rapid initial expansion and the period of arrested expansion. At intermediate times $5 \lesssim t \lesssim 18$ ($2t_F \lesssim t \lesssim 7t_F$) the impurity is approximately stationary and Gaussian in shape.

2. *Behavior with variation of the interaction strength c*

How the behavior of the ladder motion of the center of mass changes with the interaction strength reveals the competition between interactions in the system and spreading of the impurity. An intuitive picture to have in mind is that of a liquid, which becomes 'stiffer' with increasing interaction strength. At first blush, such a picture may seem to be inconsistent with the presented center of mass motion (see Fig. 3 of the main text), which appears to sharpen with weakened interactions. The observed behavior can be explained as follows. When the interaction strength c is weak, the impurity spreads quickly and has almost completely delocalized by the second plateau. As a consequence, the second plateau is relatively flat and the transient region between the plateaux is broad. With strengthening interactions, the spreading of the impurity is hindered and the spreading has yet to finish by the time the second plateau is reached. The second plateau appears less stable for strong interactions as the impurity continues to slowly spread whilst approximately stationary, shifting the center of mass slightly. We give evidence for this picture in the remainder of this section.

The behavior of the center of mass motion can be seen in Fig. 3 of the main text for $c = 5, 10, 20$ (see also Fig. S6 for $c = 10$). We will first address the behavior of the transient regions and then the stability of the plateaux upon varying the interaction strength, showing that it is consistent with the intuitive picture of interactions creating a stiffer background gas. In the first transient region $t \lesssim t_F/2$ the momentum of the impurity is imparted to the fluid: this happens more quickly for stiffer (c larger) fluids. In the second transient region, the impurity is accelerated by collisions with the excitations of the background gas. The impurity immersed in the stiffer fluid is accelerated over a shorter period of time, and imparts its momentum back to the gas quicker, consistent with the intuitive picture. As a consequence, the transient region reduces in temporal extent with increasing interaction strength.

Next, we consider the behavior of the second plateaux. It is useful to consider Fig. S5; we see that the spreading of the impurity is suppressed with increasing interaction strength (this is particularly apparent in the second and fourth rows). We also see that the impurity has almost completely delocalized around the ring when $c = 5$. This is important, as the local fluctuations in the density are proportional to the local derivative of the density, and hence fluctuations are suppressed with increasing delocalization of the impurity, which improves the stability of the plateaux. Increasing the momentum of the impurity also increases the rate at which the impurity delocalizes, and the plateaux are flatter, see Fig. S7 [see also Fig. S6(b)]. Furthermore, Fig. S5 also shows that the

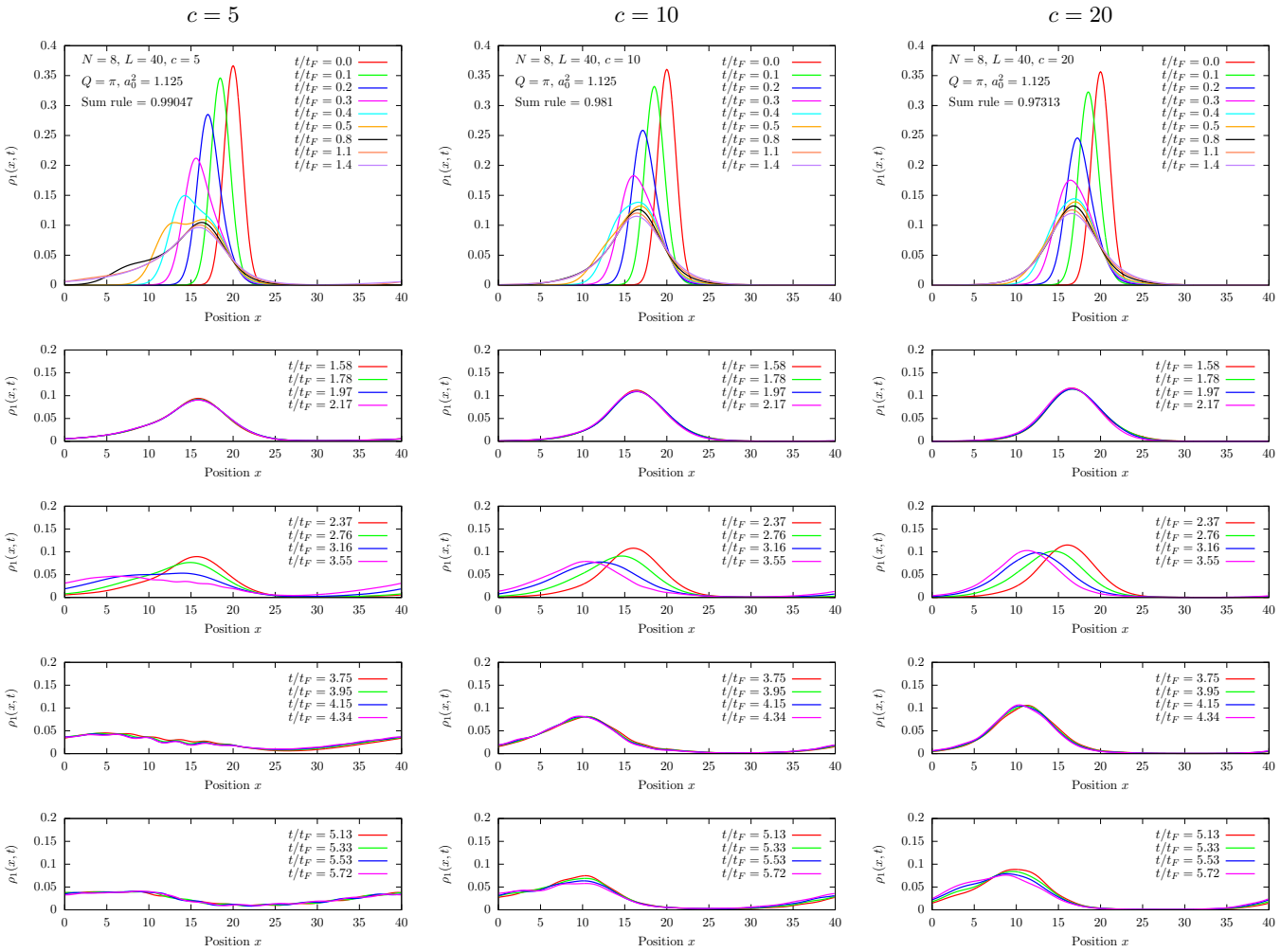

FIG. S5. Real time slices of the time-evolution of the impurity density for the three values of the interaction parameter $c = 5, 10, 20$ from the initial state with $a_0^2 = 1.125$ and $Q = \pi$.

slow drifting of the second $c = 10, 20$ plateau corresponds to small changes in the shape of the impurity, corresponding to a transfer of weight leftwards, see Fig. S8. This transfer of weight, due to the slight asymmetric spreading of the impurity, causes the drifting of the second plateau.

Delocalization of the impurity does not only increase the stability of the plateaux, it also leads to a smearing of the transient region, see Fig. 3 of the main text and Fig. S7(a). This is also consistent with our intuitive picture: excitations in the background gas now scatter on a increasingly extended object. Some excitations pass through the impurity, some scatter on the right or left of the impurity; the transient motion becomes more unclear and the transition between plateaux broadens [e.g., the peak velocity of the COM is reduced, see the inset of Fig. 3 of the main text and Fig. S7(a)].

F. The diagonal ensemble

1. *The impurity density in the diagonal ensemble*

To ascertain whether the impurity density becomes translationally invariant at long times after the impurity is injected, we compute the density profile in the diagonal ensemble

$$\rho_1(x)_{DE} = \sum_{\{k\};\mu} \sum_{\{p\};\lambda} \delta_{E_k,E_p} e^{i(K_p - K_k)x} \langle \Psi(Q)|\{p\};\lambda\rangle \times \langle\{p\};\lambda|\Psi_1^\dagger(0)\Psi_1(0)|\{k\};\mu\rangle\langle\{k\};\mu|\Psi(Q)\rangle, \tag{S6}$$

which follows from a stationary phase argument in the long time limit. Herein we assume the diagonal ensemble coincides with the long time limit. Representative results for $N = 8$ particles on the length $L = 40$ ring with interaction parameter $c = 10$ are shown in Fig. S9. There, we see that the diagonal ensemble result for the

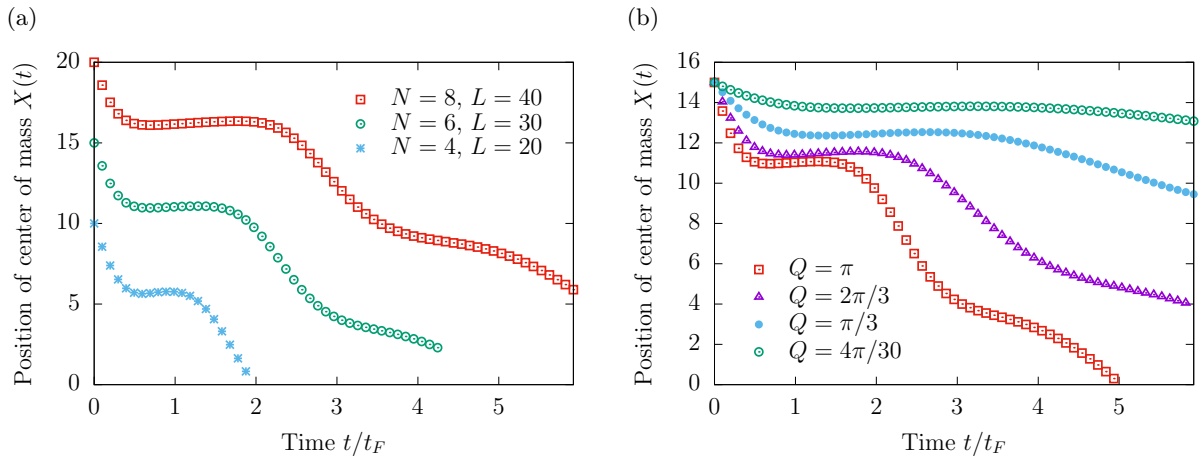

FIG. S6. Motion of the centre of mass coordinate $X(t)$ [as defined in Eq. (8)] for the initial state $|\Psi(Q)\rangle$ [defined in Eq. (4)] with $x_0 = L/2$ and $Q = \pi$ for (a) a number of system sizes L with fixed total particle density N/L and interaction strength $c = 10$; (b) a number of different initial center of mass momenta Q for $L = 30$, $N = 6$ and $c = 10$.

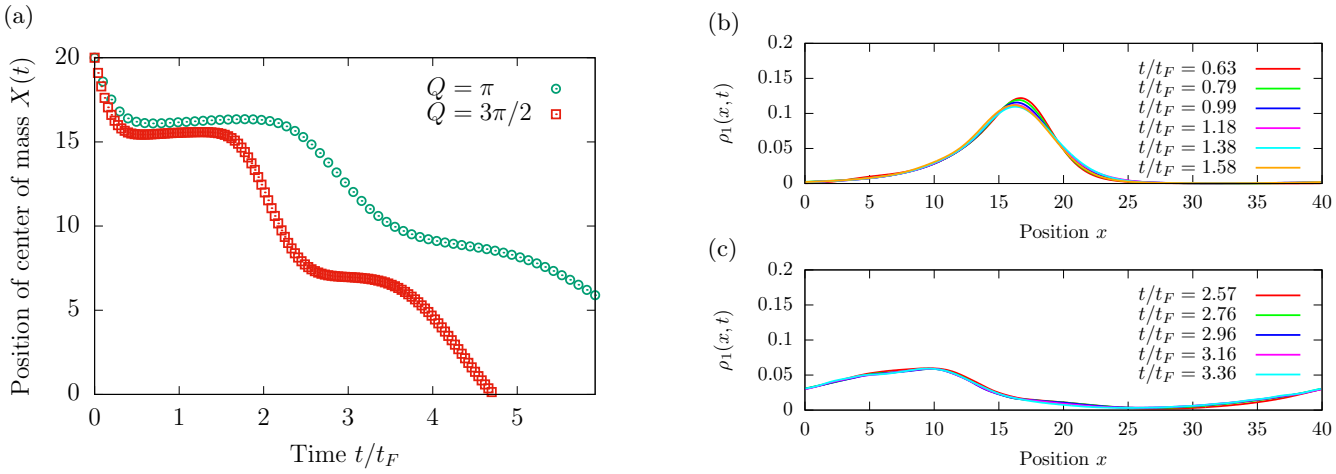

FIG. S7. (a) Motion of the center of mass of an impurity with $a_0^2 = 1.125$ and $Q = \pi,\ 3\pi/2$ for $N = 8$ particles on the length $L = 40$ ring with $c = 10$. (b) The impurity density on the (b) first and (c) second plateau for $Q = 3\pi/2$ (*cf.* the second column of Fig. S5 for $Q = \pi$).

density with initial $Q = 0$ is not translationally invariant, whilst for $Q = \pi$ the density profile appears much closer to constant. This provides strong evidence that for sufficiently large Q the impurity is almost completely delocalized around the ring in the long-time limit.

One important question raised by Fig. S9 is whether there is a sharp transition or a smooth reduction in the extent to which translational symmetry is broken with increasing Q. In Fig. S10(a) we present the impurity density in the diagonal ensemble for a number of initial momenta Q and $N = 4$ particles, and we show that the severity of the translational symmetry breaking is smoothly reduced as a Gaussian in the momentum of the initial state in Fig. S10(b). Formally, this means that translational invariance is *only recovered in the* $Q \to \infty$ *limit*. However, in a practical sense, translational symmetry is restored for sufficiently large Q for a finite precision measurement.

The origin of this Gaussian scaling can easily be explained by a degeneracy in our system: for each Bethe state $|\{k_1, k_2, \ldots, k_N\}; \mu\rangle$ there exists a state with the same energy and opposite momentum $|\{-k_1, -k_2, \ldots, -k_N\}; -\mu\rangle$. The diagonal ensemble (S6) now contains two types of terms: diagonal matrix elements which sum to $1/L$ and off-diagonal terms $\delta\rho_1(x)_{DE}$ which break translational invariance:

$$\delta\rho_1(x)_{DE} = \sum_{\{k\};\mu} \langle\Psi(Q)|\{k\};\mu\rangle\langle\{-k\};-\mu|\Psi(Q)\rangle e^{2iK_k x} \times \langle\{k\};\mu|\Psi_1^\dagger(0)\Psi_1(0)|\{-k\};-\mu\rangle + \ldots \quad \text{(S7)}$$

Here the ellipses denote other terms arising from other (possible) degeneracies. The overlap between the initial state and the Bethe states $\langle\Psi(Q)|\{k\};\mu\rangle$ is weighted by a Gaussian factor $\propto \exp(-Q^2)$. This Gaussian term will

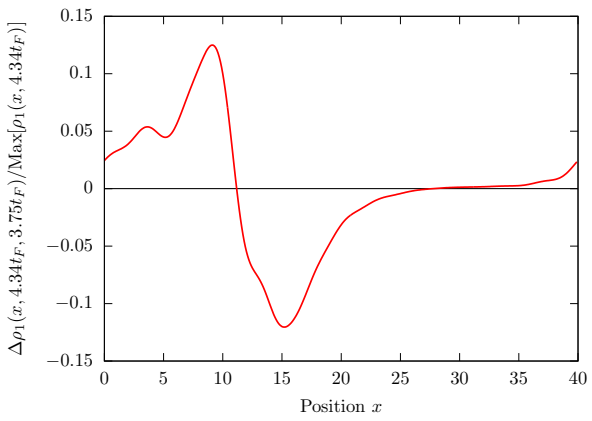

FIG. S8. The difference $\Delta\rho_1(x, t_1, t_2) = \rho_1(x, t_1) - \rho_1(x, t_2)$ in the density at times $t/t_F = 4.34$ and $t/t_F = 3.75$ for $c = 20$, see Fig. S5. We normalize to the maximum value of the density at time $t/t_F = 4.34$. A clear transfer of weight, from the right hand side of the impurity wave packet to the left with increasing time is seen, resulting in the drifting of the center of mass plateau shown in Fig. 3 of the main text.

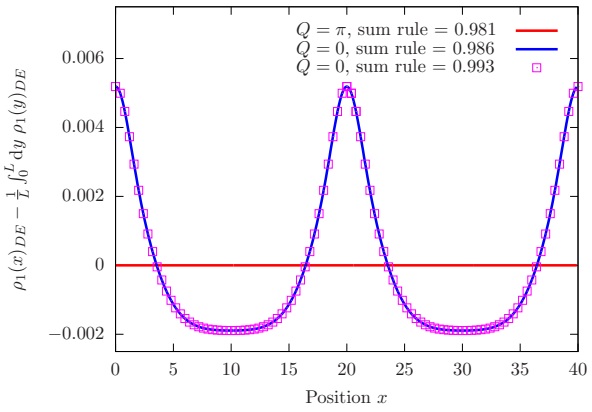

FIG. S9. Results for the impurity density in the diagonal ensemble (S6) for the initial state $|\Psi(Q)\rangle$ [defined in Eq. (4)] with momentum $Q = 0, \pi$ and $a_0^2 = 1.125$ for $N = 8$ particles on the length $L = 40$ ring with interaction parameter $c = 10$. The largest sum rule saturation requires 69532 states in each sum of Eq. (S6). Positions of the peaks are at x_0 and $x_0 + L/2$.

be present in *any terms* which break translational invariance, and hence the extent to which translational symmetry is broken is smoothly suppressed with increasing Q, as observed in Fig. S10(b).

When considering the center of mass coordinate motion, we do not see a qualitative difference for cases in which the diagonal ensemble result is (almost) translationally invariant and those in which the translational invariance is more strongly broken, see Fig. S6(b).

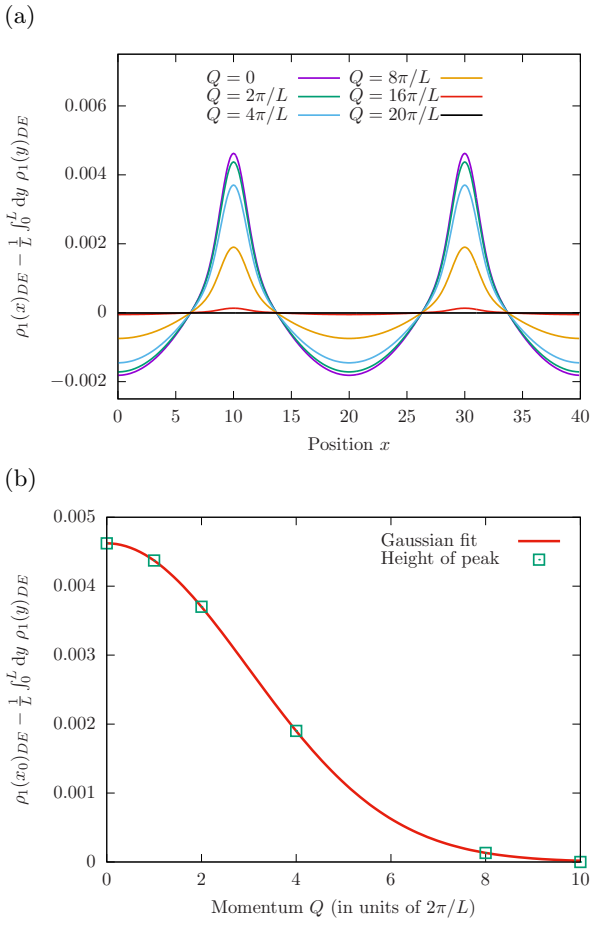

FIG. S10. (a) Deviation of expectation value of the impurity density operator in the diagonal ensemble (S6) from the translational invariant case for the initial state with momentum Q and $x_0 = L/4$. Results are for $N = 4$ particles on the ring of length $L = 40$ with interaction parameter $c = 10$; sum rules are saturated to at least 0.997 and we see now change in the extent of translational symmetry breaking with increasing saturation of the sum rule. (b) Maximum value of the deviation at $x = x_0$ as a function of Q with a Gaussian fit. Note that the peaks in (a) are shifted compared to Fig. S9 solely due the change in x_0.

2. *The momentum of the impurity in the diagonal ensemble*

Having computed the diagonal ensemble result for the density of the impurity, we now turn our attention to computation of the momentum of the impurity. We define the momentum of the impurity as

$$K(t) = \sum_p p\ \langle\Psi(Q)|e^{iHt}\Psi_{1,p}^\dagger\Psi_{1,p}e^{-iHt}|\Psi(Q)\rangle, \quad \text{(S8)}$$

where $\Psi_{1,p} = \frac{1}{L}\int \mathrm{d}x e^{-ipx}\Psi_1^\dagger(x)$ is the momentum space annihilation operator for a boson of species 1. In the $t \to \infty$ limit we assume that this is given by the diagonal ensemble and as $\Psi_{1,p}^\dagger\Psi_{1,p}$ conserves momentum, the

diagonal ensemble result is

$$K_{DE} = \sum_{\{k\};\mu} \sum_{p} p \, \langle \Psi(Q)|\{k\};\mu\rangle\langle\{k\};\mu|\Psi(Q)\rangle \times \langle\{k\};\mu|\Psi^{\dagger}_{1,p}\Psi_{1,p}|\{k\};\mu\rangle. \quad \text{(S9)}$$

Fourier transforming to real space operators, and inserting the resolution of identity over one-component Lieb-Liniger eigenstates, we find

$$K_{DE} = \sum_{\{k\};\mu} \sum_{\{q\}} \Big(K_k - K_q\Big) \times \Big|\langle \Psi(Q)|\{k\};\mu\rangle\langle\{k\};\mu|\Psi^{\dagger}(0)|\{q\}\rangle\Big|^2, \quad \text{(S10)}$$

which is expressed in terms of known matrix elements. Using the previously discussed symmetry of the Bethe states (and a similar property for the one-component states) and the properties of the matrix elements of the creation operators, we can write the momentum of the impurity in the diagonal ensemble as

$$K_{DE} \propto \sum_{\{k\};\mu} \sum_{\{q\}} \Big(K_k - K_q\Big)\Big(e^{-a_0^2(Q+K_k)^2} - e^{-a_0^2(Q-K_k)^2}\Big) \times \Big|\langle\Omega|\Psi(0)|\{k\};\mu\rangle\langle\{k\};\mu|\Psi^{\dagger}(0)|\{q\}\rangle\Big|^2 \quad \text{(S11)}$$

for the one-component ground state $|\Omega\rangle$ containing an odd number of particles. We immediately see that for $Q = 0$ the momentum of the impurity remains at zero at all times (consistent with the $Q = 0$ time-evolution).

* nrobinson@bnl.gov

[1] B. Pozsgay, W.-V. van Gerven Oei, and M. Kormos, J. Phys. A **45**, 465007 (2012).
[2] S. Pakuliak, E. Ragoucy, and N. A. Slavnov, ArXiv e-prints (2015), arXiv:1503.00546 [math-ph].
[3] B. Pozsgay, J. Stat. Mech. **2011**, P11017 (2011).
[4] V. E. Korepin, N. M. Bogoliubov, and A. G. Izergin, *Quantum Inverse Scattering Method and Correlation Functions* (Cambridge University Press, 1997).
[5] N. Reshetikhin, J. Sov. Math. **46**, 1694 (1989).
[6] G. Pang, F. Pu, and B. Zhao, J. Math. Phys. **31**, 2497 (1990).
[7] F. Göhmann and V. Korepin, Phys. Lett. A **263**, 293 (1999).
[8] N. Slavnov, Theor. Math. Phys. **82**, 273 (1990).
[9] T. Kojima, V. E. Korepin, and N. A. Slavnov, Commun. Math. Phys. **188**, 657 (1997).
[10] V. E. Korepin and N. A. Slavnov, Int. J. Mod. Phys. B **13**, 2933 (1999).